Photocurrents in Nanotube Junctions

D. A. Stewart and François Léonard
Sandia National Laboratories, Livermore, California 94551, USA
(Received 23 July 2003; revised manuscript received 14 June 2004; published 31 August 2004)

Photocurrents in nanotube *p-n* junctions are calculated using a nonequilibrium Green function quantum transport formalism. The short-circuit photocurrent displays band-to-band transitions and photon-assisted tunneling, and has multiple sharp peaks in the infrared, visible, and ultraviolet. The operation of such devices in the nanoscale regime leads to unusual size effects, where the photocurrent scales linearly and oscillates with device length. The oscillations can be related to the density of states in the valence band, a factor that also determines the relative magnitude of the photoresponse for different bands.

DOI: 10.1103/PhysRevLett.93.107401 PACS numbers: 85.60.–q, 72.40.+w, 73.63.Fg, 78.67.Ch

Carbon nanotubes (NTs) have been the subject of intensive research due to their intriguing electronic and structural properties, and have demonstrated great promise for future nanoelectronic devices [1]. However, their potential for opto-electronic applications has received much less attention, despite the ideal properties that NTs present. One desirable property of opto-electronic materials is a direct band gap, since it allows optical transitions to proceed without the intervention of phonons. NTs are unique in this aspect, since *all* the bands in *all* semiconducting NTs have a direct gap. Furthermore, the low dimensionality of NTs leads to a diverging density of states at the band edge and a high surface-to-volume ratio, reducing sensitivity to temperature variations and allowing efficient use of the material. Finally, nonradiative transitions can significantly reduce the performance of conventional materials; NTs are believed to have low defect density, reducing nonradiative transitions.

These unique properties of NTs are only starting to be explored for opto-electronics. Recent experimental work [2] has shown that NT field-effect transistors can emit polarized light, while illumination of these and other NT devices generates significant photocurrent [3,4]. Such observations have also been made in semiconductor nanowires [5–7]. Often, the observed opto-electronic effects are due to the presence of a *p-n* junction, with various physical realizations (electrostatically defined [2,3], crossed-wire geometry [6], or modulated chemical doping [7].) Modulated chemical doping of individual semiconducting single-wall NTs to create "on-tube" *p-n* junctions has recently been reported in the literature [8]. These NT *p-n* junctions serve as excellent test beds for understanding opto-electronics at reduced dimensionality.

Here we show that in simple NT *p-n* junctions, the photocurrent shows unusual features. Unlike traditional devices, the photoresponse in the NT junctions consists of multiple sharp peaks, spanning the infrared, visible, *and* ultraviolet. Furthermore, at nanoscale dimensions, the NT junctions show size effects, where the photocurrent scales and oscillates with device length.

We consider a NT *p-n* junction under illumination, as shown in Fig. 1. We use a (17,0) single-wall, semiconducting NT of radius 0.66 nm, and model the doping as in Ref. [9]. Our tight-binding Hamiltonian with one π orbital per carbon atom and nearest-neighbor matrix element of $\gamma = 2.5$ eV gives a direct band gap for this NT of 0.55 eV. The incident light is assumed to be monochromatic, with polarization parallel to the NT axis.

To calculate the photocurrent, we use a nonequilibrium Green function formalism [10] in a real-space representation. The device consists of an illuminated scattering region connected to two dark semi-infinite leads, which are also doped (17,0) NTs. The structure of the (17,0) NT corresponds to parallel rings of 17 atoms, with spacing alternating between 0.07 nm and 0.14 nm. Each ring forms a layer in our system, with the rings in the scattering region labeled from 1 to N.

Since only layers 1 and N couple with the leads, the steady-state, time-averaged current can be written as

$$I = \frac{4e\gamma}{\pi\hbar} \int dE \mathrm{Re}[G^{<}_{N+1,N} + G^{<}_{1,0}]. \qquad (1)$$

(This expression assumes that the hole current is equal and opposite to the electronic current and that the cou-

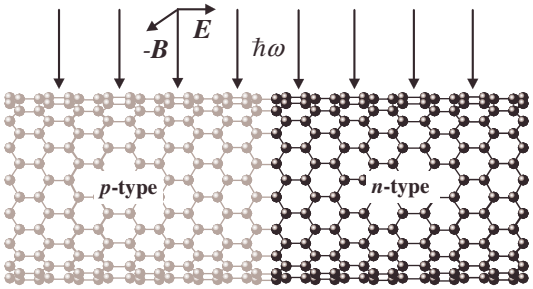

FIG. 1 (color online). Sketch of a portion of the scattering region for the (17,0) nanotube *p-n* junction. The scattering region is attached to two semi-infinite leads (not shown in figure). The incoming light of energy $\hbar\omega$ is polarized along the length of the nanotube, with electric field **E** and magnetic field **B**.

pling of layers 1 and N to the leads is γ. The appropriateness of this equation for time-dependent Hamiltonians is discussed in Ref. [11].) Here, $G^<_{N+1,N}$ and $G^<_{1,0}$ cross the scattering region boundary. To relate these terms to $G^<$ calculated entirely in the scattering region, we use the Dyson equations [12] $\gamma G^<_{1,0} = G^<_{1,1}\Sigma^R_{1,1} + \Sigma^<_{1,1}G^R_{1,1}$ and $\gamma G^<_{N+1,N} = G^<_{N,N}\Sigma^R_{N,N} + \Sigma^<_{N,N}G^{R*}_{N,N}$. (We also note that in the presence of electron-photon interactions *and* the potential step in the *p-n* junction [11], $G^<_{N+1,N} \neq G^<_{1,0}$, an equality that would normally hold for a system without inelastic scattering.)

In the scattering region, $G^<$ is determined from the equations

$$G^< = G^R\Sigma^< G^{R\dagger} \tag{2}$$

and

$$G^R = [EI - H - \Sigma^R]^{-1}, \tag{3}$$

where H is the Hamiltonian for the NT *p-n* junction under illumination. The functions Σ^R and $\Sigma^<$ represent the interaction of the scattering region with the semi-infinite (17,0) NT leads and the incident light. In the presence of the electron-photon interaction, these functions depend on $G^<$, and the equations are coupled and nonlinear. To simplify the calculation, we perform an expansion to first order in the light intensity: $G^< = G^{<0} + G^{<(ph)}$, $G^R = G^{R0} + G^{R(ph)}$, $\Sigma^< = \Sigma^{<0} + \Sigma^{<(ph)}$, and $\Sigma^R = \Sigma^{R0} + \Sigma^{R(ph)}$, where the order zero functions represent the dark *p-n* junction. In the absence of an applied bias, the only current in the device is the photocurrent

$$I^{(ph)} = \frac{4e\gamma}{\pi\hbar}\int dE \mathrm{Re}[G^{<(ph)}_{N+1,N} + G^{<(ph)}_{1,0}], \tag{4}$$

where

$$G^{<(ph)} = G^{R0}\Sigma^{<(ph)}G^{R0\dagger} + G^{R0}\Sigma^{R(ph)}G^{R0}\Sigma^{<0}G^{R0\dagger} + G^{R0}\Sigma^{<0}(G^{R0}\Sigma^{R(ph)}G^{R0})^\dagger. \tag{5}$$

Here, $G^{R0} = [EI - H_0 - \Sigma^{R0}]^{-1}$, with the Hamiltonian matrix elements $H_0^{2l,2l-1} = H_0^{2l-1,2l} = 2\gamma\cos(\frac{\pi J}{M})$, $H_0^{2l,2l+1} = H_0^{2l+1,2l} = \gamma$, and $H_0^{l,l} = -eV_l$, where V_l is the electrostatic potential on layer l. The self-energies Σ^{R0} due to the semi-infinite leads are calculated using a standard iterative approach [13], and $\Sigma^{<0} = -2f\mathrm{Im}\Sigma^{R0}$ where f is the Fermi function. The electrostatic potential and charge distribution are determined using a self-consistent procedure as in Ref. [9]. (Including electron-hole recombination and other multiphoton processes requires going beyond the perturbation scheme introduced here, and is beyond the scope of this Letter. At low light intensities, our calculations should provide a reasonable approximation.)

To derive the functions $\Sigma^{<(ph)}$ and $\Sigma^{R(ph)}$ due to the electron-photon interaction, we use the interaction Hamiltonian $H_{el-ph} = \frac{e}{m}\mathbf{A}\cdot\mathbf{p}$ where $\mathbf{A}$ is the time-dependent electromagnetic vector potential, $\mathbf{p}$ is the electronic momentum operator, and m is the electron mass. Following the procedure of Ref. [14], we obtain

$$\Sigma^{\{R,<\}(ph)}_{lm}(E) = \alpha\sum_{pq} P_{lp}P_{qm}G^{\{R,<\}0}_{pq}(E - \hbar\omega) \tag{6}$$

with

$$P_{lm} = \delta_{l\pm1,m}\left[f^\pm(l) + f^\pm(m)\cos\left(\frac{\pi J}{M}\right)\right]. \tag{7}$$

In these equations, $f^\pm(l) = \mp 1 - (-1)^l$, $\alpha = \frac{e^2a^2\gamma^2F}{2\hbar\omega c\varepsilon}$ with $a = 0.07$ nm the smallest ring separation, $\hbar\omega$ the photon energy, c the speed of light, and ε the permittivity of free space. J is the circumferential angular momentum, labeling each of the $M = 17$ bands of the NT. Conservation of J is enforced, as required for light polarization parallel to the tube axis [15]. Since the photocurrents calculated in this work are proportional to the photon flux F, we focus on the photoresponse $I^{(ph)}/eF$.

Figure 2(a) shows the calculated self-consistent band diagram for the NT *p-n* junction for a doping of 5×10^{-4} electrons/C atom. The figure shows the conduction and valence band edges of the band with the smallest band gap, $J = 6$, shifted by the local electrostatic poten-

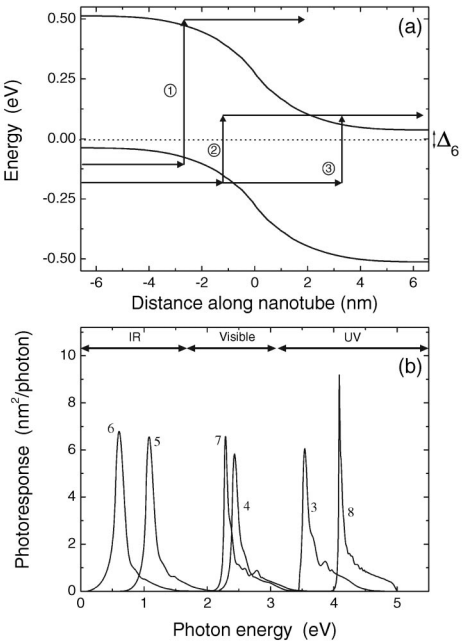

FIG. 2. Panel (a) shows the calculated self-consistent band bending for the NT *p-n* junction. Solid lines are the valence and conduction band edges for the $J = 6$ band. Dotted line is the Fermi level. Path 1 represents a band-to-band transition while paths 2 and 3 represent photon-assisted tunneling. Panel (b) shows the photoresponse for this device, plotted for each band J (labeled with the value of J in the figure).

tial. The band bending is characterized by a step at the junction and flat bands away from the junction region [16].

The calculated photoresponse for this device at zero bias when 128 rings are illuminated is shown in Fig. 2(b). The photoresponse due to bands $J = 6, 5, 7, 4, 3, 8$ (increasing band gap) is separately plotted in the figure (bands 11, 12, 10, 13, 14, 9 are equivalent). The general trend is for the photoresponse for the different bands to peak at higher photon energies as the band gap increases. Because the scattering cross section decreases with $\hbar\omega$ [the $(\hbar\omega)^{-1}$ factor in Eq. (6)], one would expect the maximum photoresponse attained for each band to decrease with band gap. Surprisingly, the height of the peaks in Fig. 2(b) does not follow this behavior; in particular, the response for band $J = 8$ is actually larger than the response for band $J = 6$. This is a result of the different bands having different effective masses. Indeed, the effective mass for $J = 8$ is about 36 times larger than for $J = 6$, leading to a much larger density of states near the edge of the valence band. (The role of the density of states will be discussed further below.)

Path 1 in Fig. 2(a) shows a band-to-band transition with the absorption of a photon of energy $\hbar\omega = 0.6$ eV. An electron coming from the p-type side of the device in the valence band absorbs a photon and is excited to the conduction band, where it then continues to the n-type terminal. Such a transition is allowed when the photon energy exceeds the band gap E_g (0.55 eV for band 6). Band-to-band photocurrents in the NT device in the left lead, due to electrons coming from the n-type terminal, vanish unless the photon energy is larger than the band gap plus the potential step across the junction, $\hbar\omega \gtrsim 1$ eV in Fig. 2(b). This asymmetry in the currents to the left and right terminals leads to the net photocurrents in Fig. 2(b).

While these band-to-band transitions explain part of the photoresponse, a significant response exists at energies below the band gap. Such contributions can be attributed to photon-assisted tunneling. Paths 2 and 3 in Fig. 2(a) show two possible paths for photon-assisted tunneling. For a given band J, this process can only occur when $\hbar\omega > \Delta_J$, where Δ_J is the difference between the asymptotic conduction band edge on the p-type side and the asymptotic valence band edge on the n-type side (equal to 0.06 eV for the $J = 6$ band shown in Fig. 2(a)). The photon-assisted tunneling thus turns on at $\hbar\omega = \Delta_J$. As the photon energy increases above Δ_J, more states in the band gap become available for transport, and the photoresponse increases. For the bands with larger band gaps, the tail due to photon-assisted tunneling is less important relative to the band-to-band peak, since tunneling probabilities decrease with band gap.

The photoresponse of the different bands leads to multiple sharp peaks in three different regions of the electromagnetic spectrum: infrared, visible, and ultraviolet. This unusual behavior arises because all the bands in the NT have a direct band gap, which leads to a response over a wide energy spectrum. The separation of this wide response into peaks grouped in different regions of the electromagnetic spectrum is due to the particular electronic band structure of the NT, which has groups of bands separated by relatively large energies. The conduction band edges for $J = 6$ and $J = 5$ (infrared response) are separated from those of bands 4 and 7 (visible response) by about 0.6 eV, which are in turn separated by about 0.5 eV from the $J = 3$ and $J = 8$ conduction band edges (ultraviolet response).

In conventional bulk junctions, the photoresponse depends only on the dimensions of the device *perpendicular* to current flow. The nanotube device, however, shows a dependence with *length*, as shown in Fig. 3. Clearly, for $\hbar\omega = 0.4$ eV (photon-assisted tunneling) the photoresponse saturates with length, due to the fact that the wave functions in the band gap decay exponentially away from the junction. The response for $\hbar\omega = 0.612$ eV and $\hbar\omega = 0.7$ eV shows a completely different behavior, oscillating around a general linear increase.

These surprising results can be understood from a simplified description of the photocurrent in the nanotube. The photocurrent flowing to the right lead can be expressed as $I_R^{(ph)} = \frac{2e}{\pi\hbar} \int i_R(E)dE$ with

$$i_R(E) = -c_f \Gamma_R \mathrm{Im}(G^{R0} \Sigma^{<(ph)} G^{R0\dagger})_{NN}, \qquad (8)$$

where $\Gamma_R = -2\mathrm{Im}\Sigma_{NN}^{R0}$ and $c_f = 1 - \frac{f(E)}{f(E-hw)}$ reflects the first order correction to the zero bias electron population in the conduction band due to $\Sigma^{R(ph)}$. [Eq. (8) can be obtained from Eq. (1) by using Dyson's equation $\gamma G_{N+1,N}^{<} = G_{N,N}^{<} \Sigma_{N,N}^{R} + \Sigma_{N,N}^{<} G_{N,N}^{R*}$, the relation $G_{i,j}^{<} = -G_{j,i}^{<*}$, and the condition that the net current must vanish

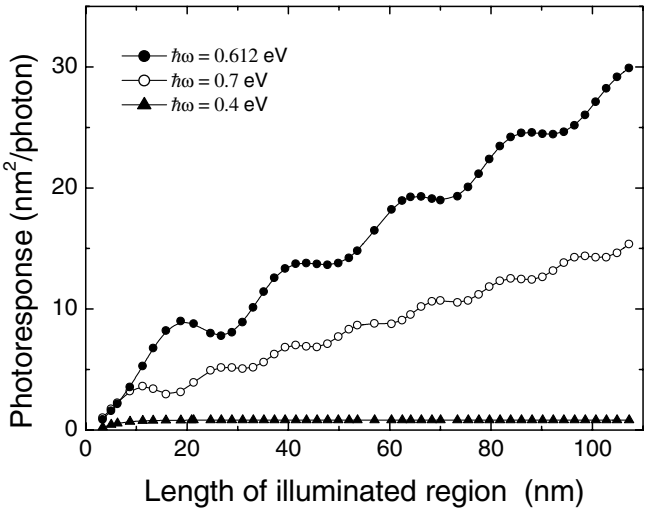

FIG. 3. Dependence of the photoresponse on the length of the illuminated region, for different photon energies.

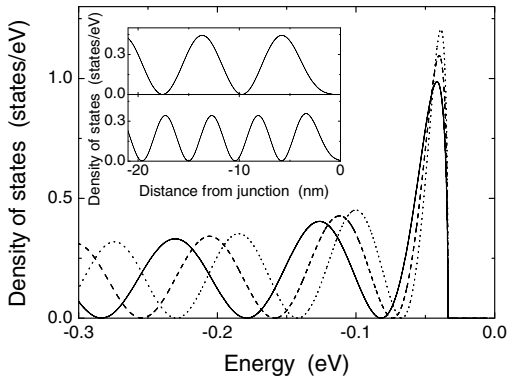

FIG. 4. Density of states at layer 11 as a function of energy. Solid, dashed, and dotted lines are for illumination lengths of 24.78, 26.88, and 28.98 nm, respectively. The top (bottom) inset shows the density of states on the even rings at energy -0.1 eV (-0.2 eV).

for the dark junction at zero bias.] At zero bias, $G^{<0}$ is purely imaginary, and therefore so is $\Sigma^{<(ph)}$. The above equation becomes

$$i_R(E) = -c_f \Gamma_R \sum_{k,p} \mathrm{Im}\Sigma^{<(ph)}_{kp} \mathrm{Re}(G^{R0}_{Nk} G^{R0*}_{Np}). \qquad (9)$$

For a given outgoing electron energy E and photon energy $\hbar\omega$, we have found numerically that the argument of the summation is peaked around the diagonal $k = p$. Taking only these contributions, we obtain

$$i_R(E) \sim -c_f \Gamma_R \sum_{k} \mathrm{Im}\Sigma^{<(ph)}_{kk} |G^{R0}_{Nk}|^2. \qquad (10)$$

The photocurrent in the NT can thus be understood in terms of the excitation of electrons in each layer k along the NT (the $\mathrm{Im}\Sigma^{<(ph)}_{kk}$ term in the above equation), and the subsequent transmission to the lead by G^{R0}_{Nk}.

To explain the linear scaling, we note that for $\hbar\omega > E_g$ and $E > E_c^{-\infty}$ where $E_c^{-\infty}$ is the asymptotic value of the conduction band edge on the p-type side of the device, there is a section of the NT where band-to-band transitions are allowed, and the sum in the last equation is dominated by this section of the NT. As the length of the illumination region is increased, a longer section of the NT is available for band-to-band transitions, leading to the linear scaling of the current with length.

The photoresponse oscillations and dependence on the effective mass can be understood by noting that $\mathrm{Im}\Sigma^{<(ph)}_{kk}(E)$ contains terms like $\mathrm{Im}G^{<0}_{kk}(E - \hbar\omega)$, which are related to the density of states at layer k, D_k, through $\mathrm{Im}G^{<0}_{kk}(E - \hbar\omega) = \pi f(E - \hbar\omega) D_k(E - \hbar\omega)$. Therefore, the photocurrent is sensitive to the density of states at energy $E - \hbar\omega$. This explains the origin of the dependence on the effective mass, and the relative height of the peaks in Fig. 2(b).

Figure 4 shows the valence band density of states for $J = 6$ calculated at layer 11 for systems with illuminated lengths of 24.78, 26.88, and 28.98 nm. (This is the density of states near the edge of the illuminated region, which is moving further away from the junction as the length increases.) The density of states contains many peaks, and as the system size changes, the peaks move in energy. Because the propagator $|G^{R0}_{Nk}|^2$ is sharply peaked at energy $E_c^{-\infty}$, the photoresponse is particularly sensitive to the density of states at $E_c^{-\infty} - \hbar w$. At that energy, the density of states oscillates as a function of the distance from the p-n junction, as illustrated in the inset of Fig. 4. This leads to the oscillations in the photoresponse as a function of illumination length shown in Fig. 3. The oscillation wavelength of the density of states increases for energies closer to the band edge, causing the different oscillation wavelengths for $\hbar w = 0.612$ eV and $\hbar w = 0.7$ eV in Fig. 3.

Although the device presented here is fairly simple, it already shows the richness of new phenomena that arises in nanoscale opto-electronics. One may envision several uses for this or related devices (photodetection, power generation, optical communication, etc.), but the important point is that the behavior is much different from traditional devices and must be taken into account in future device development.

Work supported by the Office of Basic Energy Sciences, Division of Materials Sciences, U.S. Department of Energy under Contract No. DE-AC04-94AL85000.

[1] A. Bachtold *et al.*, Science **294**, 1317 (2001); M. S. Fuhrer *et al.*, Science **288**, 494 (2000); J. Kong *et al.*, Science **287**, 622 (2000).
[2] J. A. Misewich *et al.*, Science **300**, 783 (2003).
[3] M. Freitag *et al.*, Nano Lett. **3**, 1067 (2003).
[4] O. M. Castellini *et al.* (to be published).
[5] J. Wang *et al.*, Science **293**, 1455 (2001).
[6] X. Duan *et al.*, Nature (London) **409**, 66 (2001).
[7] M. S. Gudiksen *et al.*, Nature (London) **409**, 66 (2002).
[8] C. Zhou *et al.*, Science **290**, 1552 (2000).
[9] F. Léonard and J. Tersoff, Phys. Rev. Lett. **85**, 4767 (2000).
[10] S. Datta, *Electronic Transport in Mesoscopic Systems* (Cambridge University Press, Cambridge, England, 1995).
[11] S. Datta and M. P. Anantram, Phys. Rev. B **45**, 13761 (1992).
[12] R. Lake *et al.*, J. Appl. Phys. **81**, 7845 (1997).
[13] M. P. Lopez-Sancho, J. M. Lopez-Sancho, and J. Rubio, J. Phys. F. Met. Phys. **15**, 851 (1985).
[14] L. E. Henrickson, J. Appl. Phys. **91**, 6273 (2002).
[15] I. Božović, N. Božović, and M. Damnjanović, Phys. Rev. B **62**, 6971 (2000).
[16] F. Léonard and J. Tersoff, Phys. Rev. Lett. **83**, 5174 (1999).